Stability analysis of magnetization in a perpendicular magnetic layer driven by spin Hall effect

Zai-Dong Li(李再东)[1,2,†], Xin-Xin Zhao(赵欣欣)[1], and Tian-Fu Xu(徐天赋)[3]

[1] *Tianjin Key Laboratory of Quantum Optics and Intelligent Photonics, School of Science, Tianjin University of Technology, Tianjin* 300384, *China*
[2] *Department of Applied Physics and School of Information Engineering, Hebei University of Technology, Tianjin* 300401, *China*
[3] *College of Science, Yanshan University, Qinhuangdao* 066004, *China*

(Received 17 October 2022; revised manuscript received 10 December 2022; accepted manuscript online 11 January 2023)

We investigate the stability of magnetization in free layer where the spin torque is induced by the spin Hall effect. In terms of the Landau–Liftshitz–Gilbert equation, we find the low-energy and high-energy equilibrium states, as well as the saddle points. The stability region is defined in the phase diagram spanned by the current density and the spin Hall angle. The spin Hall effect makes the previous saddle point into a stable state above a critical current. However, in the presence of magnetic field, the spin Hall effect leads to the opposite changes in the stable regions of the two low-energy states.

Keywords: stability, spin Hall effect, equilibrium states

PACS: 75.78.–n, 75.40.Gb, 72.25.Ba **DOI:** 10.1088/1674-1056/acb204

1. Introduction

In 1996, Slonczewski and Berger have proposed that the spin-polarized current[1] can induce the spin transfer torque effect,[2] which is an important force driving magnetization dynamics.[3–7] The spin transfer torque can be produced in spin valve structure[8] composed of a pinned layer, a spacer layer, and a free layer. The pinned layer and free layer are ferromagnetic layer, and the middle layer is nonmagnetic metal layer. When an electronic current perpendicularly propagates to the layer interface,[9] the electric current is polarized in the fixed layer and transforms its spin angular momentum to the free layer. Therefore, this case is called current-perpendicular-to-plane geometry.[10] Now, many studies have focused on the mentioned above current-perpendicular-to-plane geometry, and the corresponding spin-transfer torque has aroused people's interest with its main application prospect in the nonvolatile magnetic random access memory[11] and high frequency nanoscale microwave oscillators.[12]

Also, some experiments show that magnetization switching can also occur in current-in-plane geometry.[13–15] In this case, an in-plane current flowing into the non-magnet layer can convert into a vertical spin current by the action of spin Hall effect,[16–18] in which the spin Hall angle is the ratio of the spin current density and the charge current density. A spin current flows vertically into the ferromagnet layer interface and converts its angular momentum to the free layer, and exerts a spin torque to the free layer magnetization as the same as the current-perpendicular-to-plane geometry. It is well known that the dynamics of magnetization in the ferromagnetic layer can be described by the Landau–Liftshitz–Gilbert equation. In terms of this equation the linear stability analysis is a useful tool to build phase diagram boundary and can get the switching current[19,20] in different magnetic state.[21–28] Also, it can predict the conditions in different systems without relying on the integrability of equations.[29–32] In this paper, we study the linear stability analysis of magnetization in free layer where the spin torque[33,34] induced by the spin Hall effect. All the possible equilibrium states and their stability conditions have been obtained by the oscillations ansatz in detail, the stable and unstable regions are given in the phase diagram as well. Stability studies are fundamental significance to understand magnetization dynamics and related phenomenology. We find that the system is unstable in a strong field environment due to the magnetic switch induced by the Gilbert damping. On the other hand, it is metastable in weak field state and small particle size. The present method and results can also be extended to various frontiers of physics, including magnetic skyrmions and other topological spin structures. The local injection of spin-polarized current can be used to promote the nucleation of skyrmions, due to partial compensation of magnetization.[35] It is reported that magnetic skyrmions is a topology protected magnetic structure, which can be used as a low energy consumption and efficient information storage device.[36–38]

2. Model

As described in Fig. 1, we consider a magnetic bi-layer structure, which composed of a ferromagnetic metallic layer and a nonmagnetic metallic layer. The film lies in x–y plane. For the in-plane free layer structure, due to the spin Hall effect, the in-plane charge current running in the x direction generates the spin current running in the z direction, i.e., there exists a

[†]Corresponding author. E-mail: lizd@email.tjut.edu.cn

© 2023 Chinese Physical Society and IOP Publishing Ltd

vertical spin current under the spin Hall effect. This perpendicular spin current flows into the ferromagnet layer and transfers its spin-angular-momentum, thus, a spin Hall effect torque can be generated.

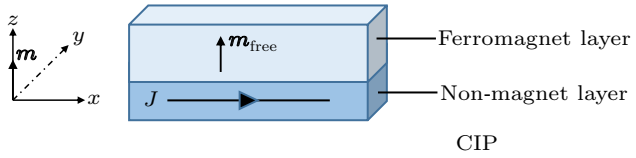


Fig. 1. Schematic drawing of the magnetic multilayers with a spin torque induced by spin Hall effect and coordinate system.

In order to study the stability of magnetization with spin Hall effect torque, we analyze the dimensionless form of the Landau–Liftshitz–Gilbert equation[39–41]

$$\frac{\partial \boldsymbol{m}}{\partial \tau} = -\boldsymbol{m}\times\boldsymbol{h}_{\text{eff}} + \alpha\boldsymbol{m}\times\frac{\partial \boldsymbol{m}}{\partial \tau} + c_j\boldsymbol{m}\times(\boldsymbol{m}\times\hat{\boldsymbol{y}}), \quad (1)$$

where $\boldsymbol{m}$ is the unit vector of ferromagnet, α is the Gilbert damping parameter, $\tau = \gamma M_s t$ is the characteristic time with M_s being the saturation magnetization, γ is the gyromagnetic ratio. The effective field $\boldsymbol{h}_{\text{eff}} = \boldsymbol{h}_k + \boldsymbol{h}$ is an effective magnetic field, which includes an effective perpendicular anisotropy field $\boldsymbol{h}_k = km_z\hat{\boldsymbol{z}}$, $k = K/\left(\mu_0 M_s^2\right)$ being the uniaxial anisotropic constant with saturation magnetization M_s, and an external field $\boldsymbol{h} = h_y\hat{\boldsymbol{y}}$. The third term in the right of Eq. (1) is the spin torques induced by the spin Hall effect, and $c_j = (\hbar/2e)/(\theta_{\text{SH}}J/(M_s d))$, where e is electron charge, θ_{SH} is an effective spin Hall angle of the system, and J is the current density in heavy metal layer, and d is the thickness of ferromagnet layer.

In this paper, we use the coherent rotational model.[42,43] Coherent mode can only occur in materials composed of small particles, where exchange coupling exceeds anisotropic energy. For larger grains, incoherent nucleation[43,44] mode is dominant. The concept of effective anisotropy has good physical significance only when the nuclear mode is regarded as coherent rotation. Where the Stoner–Wohlfarth model[45] is the most promising time independent model so far, and it is based on the coherent rotation of magnetic moment of single domain grains relative to their easy axis. Under an uniaxial anisotropic case, the dynamics of $\boldsymbol{m}$ can be described by the polar angle θ and the azimuthal angle ϕ in the spherical coordinate. Then, Eq. (1) reduces to two coupled equations

$$\begin{aligned}\dot{\theta} + \alpha\dot{\phi}\sin\theta &= h_y\cos\phi - c_j\cos\theta\sin\phi,\\ \dot{\phi}\sin\theta - \alpha\dot{\theta} &= \frac{k}{2}\sin 2\theta - c_j\cos\phi - h_y\cos\theta\sin\phi,\end{aligned} \quad (2)$$

where $\dot{\theta}$ and $\dot{\phi}$ are the time derivatives of θ and ϕ, respectively. Let $\dot{\theta} = 0$ and $\dot{\phi} = 0$, we obtain the equilibrium equation of the equilibrium magnetization states (θ_0, ϕ_0)

$$\begin{aligned}h_y\cos\phi_0 - c_j\cos\theta_0\sin\phi_0 = 0,\\ k\sin\theta_0\cos\theta_0 - c_j\cos\phi_0 - h_y\cos\theta_0\sin\phi_0 = 0.\end{aligned} \quad (3)$$

In the equilibrium states, we introduce a small perturbation to determine the stability of the equilibrium states. Substituting the ansatz $\theta = \theta_0 + \delta\theta$ and $\phi = \phi_0 + \delta\phi$ into Eq. (2) and keeping the linear terms of $\delta\theta$ and $\delta\phi$, we can get the linear equations about $\delta\theta$ and $\delta\phi$ as follows:

$$\begin{aligned}\frac{\mathrm{d}}{\mathrm{d}\tau}\delta\theta + \alpha\sin\theta_0\frac{\mathrm{d}}{\mathrm{d}\tau}\delta\phi &= k_\theta\delta\theta + k_\phi\delta\phi,\\ -\alpha\frac{\mathrm{d}}{\mathrm{d}\tau}\delta\theta + \sin\theta_0\frac{\mathrm{d}}{\mathrm{d}\tau}\delta\phi &= l_\theta\delta\theta + l_\phi\delta\phi,\end{aligned} \quad (4)$$

where $k_\theta = c_j\sin\theta_0\sin\phi_0$, $k_\phi = -h_y\sin\phi_0 - c_j\cos\theta_0\cos\phi_0$, $l_\phi = c_j\sin\phi_0 - h_y\cos\theta_0\cos\phi_0$, and $l_\theta = k\cos(2\theta_0) + h_y\sin\theta_0\sin\phi_0$.

In order to understand the stability of the equilibrium states, we assume a small periodic oscillation signal $\delta\theta$ and $\delta\phi$, where $\delta\theta = \Delta\theta\,\mathrm{e}^{\mathrm{i}\omega t}$ and $\delta\phi = \Delta\phi\,\mathrm{e}^{\mathrm{i}\omega t}$ with $\Delta\theta$ and $\Delta\phi$ being the small amplitude, respectively. Then, from Eq. (4) one gets the dispersive equation

$$\begin{vmatrix} \mathrm{i}\omega - k_\theta & \alpha\mathrm{i}\omega\sin\theta_0 - k_\phi \\ -\alpha\mathrm{i}\omega - l_\theta & \mathrm{i}\omega\sin\theta_0 - l_\phi \end{vmatrix} = 0. \quad (5)$$

Therefore, we have

$$\omega = \frac{1}{2\kappa}\left(\mathrm{i}a \pm \sqrt{b}\right), \quad (6)$$

where $\kappa = \left(1+\alpha^2\right)\sin\theta_0$, $a = (\alpha l_\theta - k_\theta)\sin\theta_0 - \alpha k_\phi - l_\phi$, and $b = 4\kappa\eta - a^2$ with $\eta = k_\theta l_\phi - k_\phi l_\theta$. From Eq. (6) we have a stable state for $a/\kappa \geq 0$ and $b \geq 0$, while the equilibrium state is unstable for the case $a/\kappa < 0$ and $b > 0$, or the case $b < 0$.

3. Stability of magnetization dynamics with spin Hall effect

In this section, we start to discuss the stability of magnetization dynamics under the different condition. According to Eqs. (3) and (6), we consider the stability analysis of magnetization with the spin Hall effect. We research the stability of the equilibrium state, and study the stable state of the equilibrium state relies on $b \geq 0$ and $a/\kappa \geq 0$.

According to Eq. (3), we get the equilibrium equation without the external magnetic field

$$c_j\cos\theta_0\sin\phi_0 = 0, \quad k\sin 2\theta_0 - 2c_j\cos\phi_0 = 0. \quad (7)$$

By solving Eq. (7) we find six equilibrium states. There are two equilibrium states with the low energy expressed by $\theta_0 = \arcsin\sqrt{(k-f_0)/(2k)}$, $\phi_0 = 0$, π, in which $f_0 = \sqrt{k^2 - 4c_j^2}$. The two equilibrium states with the high energy take the form of $\theta_0 = \arcsin\sqrt{(k+f_0)/(2k)}$, $\phi_0 = 0$, π. It is commonly recognized that $\theta_0 = 0$, π is low energy state and $\theta_0 = \pi/2$ is high

energy state in a ferromagnetic with perpendicular anisotropy. The last two equilibrium states belong to the case of saddle points (without spin Hall effect) which can be depicted as $\theta_0 = \pi/2$, $\phi_0 = \pi/2$, $3\pi/2$. Now, we begin to analyze the stability of these six equilibrium states, as shown in the phase diagram.

3.1. Stability of the high energy equilibrium states

In this section, we will investigate the stability of the high energy equilibrium states. Substituting $\phi_0 = 0$ and $\theta_0 = \arcsin((k+f_0)/(2k))^{1/2}$ into the stability condition in Eq. (6), we have $k_\theta = 0$, $k_\phi = -c_j\cos\theta_0$, $l_\theta = k\cos 2\theta_0$, $l_\phi = 0$, $\kappa = (1+\alpha^2)((k+f_0)/(2k))^{1/2}$, $a = \alpha(k-3f_0)\sqrt{k+f_0}/(2\sqrt{2k})$, and $b = \alpha^2(3c_j^2-k^2)/2 - (c_j^2(8-\alpha^2)/(2k) + (\alpha^2 k)/2)f_0$. The stability condition $a/\kappa \geq 0$ demands $c_j^2 \geq 2k^2/9$, while $b \geq 0$ demands $c_j^2 \geq k^2/3$ and $c_j^2 \leq k^2/4$, owing the relation that the second term $-(c_j^2(8-\alpha^2)/(2k) + k\alpha^2/2)f_0$ of b is negative. By comparing the condition $c_j^2 \leq k^2/4$ and $c_j^2 \geq k^2/3$, there is no common region. For another high energy equilibrium state $\theta_0 = \arcsin((k+f_0)/(2k))^{1/2}$, $\phi_0 = \pi$, we have the same result. These results denote that no stable condition for the high energy equilibrium states.

3.2. Stability of the low energy equilibrium states

Firstly, we consider the stability of the low energy of the equilibrium state $\theta_0 = \arcsin(k - f_0/(2k))^{1/2}$, $\phi_0 = 0$. Substituting θ_0, ϕ_0, and $c_j = k/2\sin 2\theta_0$ into the conditions of stability in Eq. (6), we have $k_\theta = 0$, $k_\phi = -c_j\cos\theta_0$, $l_\theta = k\cos 2\theta_0$, and $l_\phi = 0$. With these results we obtain $a = \alpha(k+3f_0)\sqrt{k-f_0}/\sqrt{8k}$, $b = \alpha^2(3c_j^2-k^2)/2 - f_0(c_j^2(8-\alpha^2)/(2k) + \alpha^2 k/2)$, and $\kappa = (1+\alpha^2)(k - f_0/(2k))^{1/2}$. In order to satisfy the stability condition $a/\kappa \geq 0$ and $b \geq 0$ it demands $|c_j| \leq k/2$ and $|c_j| \leq \sqrt{2}k\alpha/(2\zeta_2 + \alpha\zeta_1)$, where $\zeta_1 \equiv \sqrt{\alpha_1+1}$, $\zeta_2 \equiv \sqrt{\alpha_1-1}$ with $\alpha_1 \equiv \sqrt{1+\alpha^2}$. Considering $\alpha < 1$ we obtain that the stable region is satisfied by the condition $|c_j| \leq \sqrt{2}k\alpha/(2\zeta_2 + \alpha\zeta_1)$. With the definition $c_j = (\hbar/2e)/(\theta_{\rm SH}J/(\mu_0 M_s^2 d))$ we find the stable region for the equilibrium state, i.e., $\theta_0 = \arcsin(k - f_0/(2k))^{1/2}$ and $\phi_0 = 0$, demands the current density condition $|J| \leq \sqrt{2}\alpha k e d/(\hbar\theta_{\rm SH}(\zeta_2 + \alpha\zeta_1/2))$. For another low energy equilibrium state $\theta_0 = \arcsin(k - f_0/(2k))^{1/2}$, $\phi_0 = \pi$, we have the same current density condition, while we use the relation $\sin 2\theta_0 = -2c_j/k$.

With the above analysis, the stability of the equilibrium states can be represented graphically in the phase diagram in the plane of the current density J and the spin Hall angle $\theta_{\rm SH}$, as shown in Fig. 2. Here, we take the related parameters as follows: the saturation magnetization $M_s = 8.0\times10^5$ A/m, the Gilbert damping parameter $\alpha = 0.2$, the electron charge $e = 1.6\times10^{-19}$ C, the vacuum permeability $\mu_0 = 4\pi\times10^{-7}$, and $K = 1.6\times10^5$ J/m^3. Thus, the uniaxial anisotropic constant is $k = K/(\mu_0 M_s^2) \approx 0.2$, the thickness of the ferromagnet layer $d = 3$ nm. In Fig. 2 the red and cyan lines denote the boundary of $a/\kappa = 0$, and $b = 0$. Because the red and cyan lines are so close, we inset figure to distinguish the two lines. Therefore, the stable region is shown in Fig. 2 for the low energy of the equilibrium states $\theta_0 = \arcsin(k - f_0/(2k))^{1/2}$ and $\phi_0 = 0, \pi$.

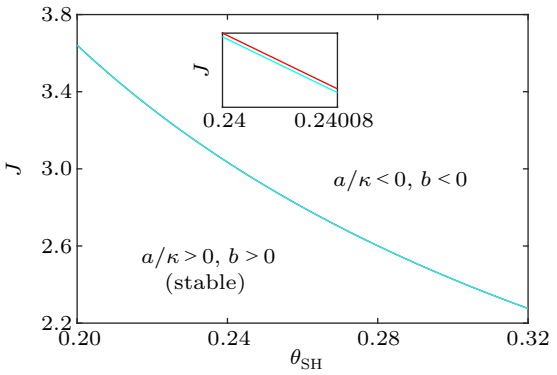


Fig. 2. The phase diagram in the J–$\theta_{\rm SH}$ plane for the stability of the equilibrium states $\theta_0 = \arcsin(k - f_0/(2k))^{1/2}$ and $\phi_0 = 0$, π. The red line and cyan line (see inset figure) denote the boundary $a/\kappa = 0$ and $b = 0$, respectively. The parameter J is in units of 10^{12} A/m^2. The other parameters are as follows: the saturation magnetization $M_s = 8.0\times10^5$ A/m, the Gilbert damping parameter $\alpha = 0.2$, the electron charge $e = 1.6\times10^{-19}$ C, the vacuum permeability $\mu_0 = 4\pi\times10^{-7}$, the reduced Planck constant $\hbar = h/2\pi$, Planck constant $h = 6.626\times10^{-34}$ J·s, $K = 1.6\times10^5$ J/m^3. Thus, the uniaxial anisotropic constant is $k = K/(\mu_0 M_s^2) \approx 0.2$, and the thickness of the ferromagnet layer is $d = 3$ nm.

3.3. Stability of the equilibrium states $(\pi/2, \pi/2)$ and $(\pi/2, 3\pi/2)$

From Eq. (1) we see that the equilibrium states $\theta_0 = \pi/2$, and $\phi_0 = \pi/2$, $3\pi/2$ form the saddle point in the absence of spin Hall effect torque, and it is unstable. However, the spin Hall effect changes the stability of these states as follows. Substituting $\theta_0 = \pi/2$, $\phi_0 = \pi/2$ into the conditions of stability in Eq. (6), we obtain $k_\theta = c_j$, $k_\phi = 0$, $l_\theta = -k$, $l_\phi = c_j$, $\kappa = 1+\alpha^2$, $\eta = c_j^2$, $a = -(\alpha k + 2c_j)$, $b = -\alpha(\alpha k^2 + 4kc_j - 4c_j^2\alpha)$. The stability conditions $a/\kappa \geq 0$ and $b \geq 0$ demand the condition $c_j \leq -\alpha k/2$, which implies the current density $J \leq -\alpha k e d/(\hbar\theta_{\rm SH})$. The same discussion gives the stability condition, which demands the current density $J \geq \alpha k e d/(\hbar\theta_{\rm SH})$ for the equilibrium states $\theta_0 = \pi/2$, and $\phi_0 = 3\pi/2$. In terms of the above analysis, the stability of the equilibrium states is $|J| \geq \alpha k e d/(\hbar\theta_{\rm SH})$, which can be represented graphically in the phase diagram in $\theta_{\rm SH}$–J plane, as shown in Fig. 3. In Fig. 3, the red and cyan lines denote as the boundary of $a/\kappa = 0$ and $b = 0$, respectively. Without the spin Hall effect, the saddle points $(\pi/2, \pi/2)$ and $(\pi/2, 3\pi/2)$ are unstable states, while the spin Hall effect drives the saddle points $(\pi/2, \pi/2)$ and $(\pi/2, 3\pi/2)$ into a stable state in the condition $|J| \geq \alpha k e d/(\hbar\theta_{\rm SH})$.

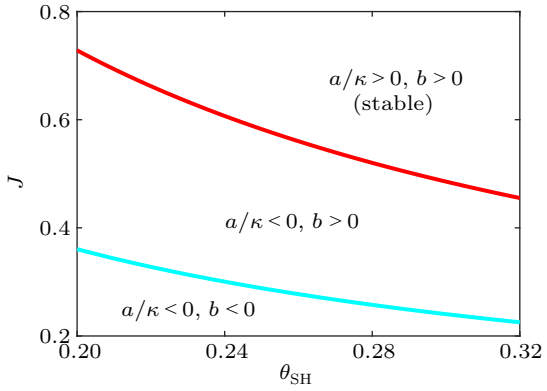


Fig. 3. The phase diagram in the J–θ_{SH} plane for the stability of the equilibrium states $(\pi/2,\ \pi/2)$ and $(\pi/2, 3\pi/2)$. The red line denotes as the boundary of $a/\kappa = 0$, the cyan line denotes as the boundary of $b = 0$. The parameters are the same as in Fig. 2.

4. Stability of magnetization dynamics with spin Hall effect and the external field

In this section, we consider the stability of magnetization dynamics with spin Hall effect and an external field $h_y\hat{\boldsymbol{y}}$, where role of the external magnetic field is similar to the field-like torque induced by spin–orbit torque (SOT) in heavy metal/ferromagnetic bilayers. The external field perpendicular to the spin current is necessary in the SOT induced magnetization switching. By solving Eq. (3) we can find four equilibrium states, i.e., $\theta_0 = \arcsin[(k \pm f_0)f_1]^{1/2}$ and $\phi_0 = \arcsin(h_y^2(k \pm f_0)k)^{1/2}/[2c_j^2(c_j^2 + h_y^2)]^{1/2}$ with $f_1 \equiv (c_j^2 + h_y^2)/(2kc_j^2)$, and $\theta_0 = \pi/2$, $\phi_0 = \pi/2,\ 3\pi/2$. It is obvious that in the absence of magnetic field these two solutions correspond to the low energy equilibrium states discussed in the previous section. In the following, we begin to analyze the stability of the above four equilibrium states and show its stable region.

Firstly, we will investigate the stability of the equilibrium state, i.e., $\theta_0 = \arcsin(\xi_1 f_1)^{1/2}$, $\phi_0 = \arcsin h_y(\xi_1 k)^{1/2}/[2c_j^2(c_j^2 + h_y^2)]^{1/2}$, where $\xi_1 = k + f_0$. Substituting θ_0 and ϕ_0 into the conditions of stability in Eq. (6) we get $k_\theta = \xi_1 h_y/(2c_j)$, $k_\phi = -\xi_2(\xi_1 f_1)^{1/2}/2$, $l_\theta = -(f_0 + \xi_1 h_y^2/2c_j^2)$, $l_\phi = h_y\xi_1(\xi_1 f_1)^{1/2}/(2c_j)$, $\kappa = (1+\alpha^2)(\xi_1 f_1)^{1/2}$, $\eta = f_0(\xi_1 h_y^2/c_j^2 - \xi_2)(\xi_1 f_1)^{1/2}/2$, and the parameters

$$
\begin{aligned}
a &= -\alpha\eta/f_0 - 2l_\phi\left[1 + \alpha c_j f_0/(h_y\xi_1)\right], \\
b &= \xi_1 f_1\Big\{2f_0\left(1+\alpha^2\right)\left(h_y^2\xi_1/c_j^2 - \xi_2\right) \\
&\quad - \left[\alpha\left(\xi_2/2 - f_0\right) - \left(1 + h_y/(2c_j)\right)h_y\xi_1\right]^2\Big\}.
\end{aligned}
$$

With the stability conditions $b \geq 0$ and $a/\kappa \geq 0$, we get the stable region in Fig. 4, in which the red line represents $a/\kappa = 0$, and the black line represents $b = 0$. The common region is represented by $b \geq 0$ and $a/\kappa \geq 0$, so the purple region is stable. From Fig. 4 we find that the spin Hall effect enlarges the stable region of this equilibrium state. Here, we select the related parameters as follows: the Gilbert damping parameter $\alpha = 0.2$, $K = 1.6 \times 10^5$ J/m^3, and then the uniaxial anisotropic constant is $k = K/(\mu_0 M_s^2) \approx 0.2$. The same stability analysis can also be discussed in detail for another equilibrium state $\theta_0 = \arcsin(\xi_2 f_1)^{1/2}$ and $\phi_0 = \arcsin h_y(\xi_2 k)^{1/2}/[2c_j^2(c_j^2 + h_y^2)]^{1/2}$. Using the relation $\cos\phi_0 = c_j\cos\theta_0\sin\phi_0/h_y$ and $\sin\phi_0 = kh_y\sin\theta_0/(c_j^2 + h_y^2)$, and substituting θ_0 and ϕ_0 into the conditions of stability in Eq. (6) we have $k_\theta = \xi_2 h_y/(2c_j)$, $k_\phi = -\xi_1(\xi_2 f_1)^{1/2}/2$, $l_\theta = f_0 - h_y^2\xi_2/(2c_j^2)$, $l_\phi = h_y\xi_2(\xi_2 f_1)^{1/2}/(2c_j)$, $\kappa = (1+\alpha^2)(\xi_2 f_1)^{1/2}$, $\eta = f_0(\xi_1 - h_y^2\xi_2/c_j^2)(\xi_2 f_1)^{1/2}/2$. The corresponding parameters are

$$
\begin{aligned}
a &= -\alpha\eta/f_0 - 2l_\phi\left[1 + \alpha c_j f_0/(h_y\xi_1)\right], \\
b &= \xi_2 f_1\Big\{2f_0\left(1+\alpha^2\right)\left(\xi_1 - h_y^2\xi_2/c_j^2\right) \\
&\quad - \left[\alpha\left(\xi_1/2 + f_0\right) - \left(1 + \alpha h_y/(2c_j)\right)h_y\xi_2\right]^2/c_j^2\Big\}.
\end{aligned}
$$

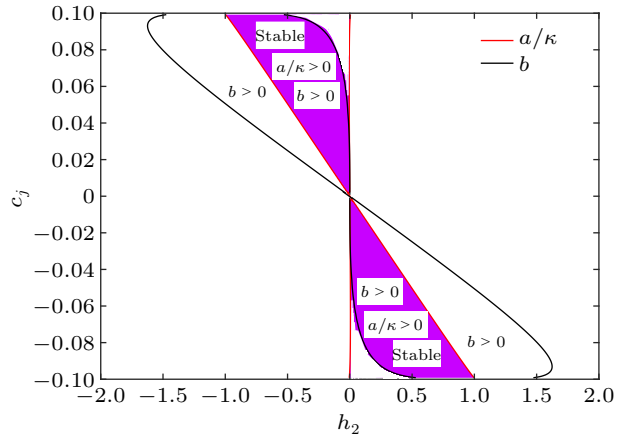


Fig. 4. The phase diagram of steady region in the h–c_j plane for the magnetic state $\theta_0 = \arcsin[(k + f_0)f_1]^{1/2}$ and $\phi_0 = \arcsin(h_2^2(k + f_0)k)^{1/2}/[2c_j^2(c_j^2 + h_2^2)]^{1/2}$. The red line denotes as the boundary of $a/\kappa = 0$, the black line denotes as the boundary of $b = 0$. The purple region denotes as the stable region. Here we select the related parameters as follows: the Gilbert damping parameter $\alpha = 0.2$, $K = 1.6 \times 10^5$ J/m^3, the uniaxial anisotropic constant is $k = K/(\mu_0 M_s^2) \approx 0.2$.

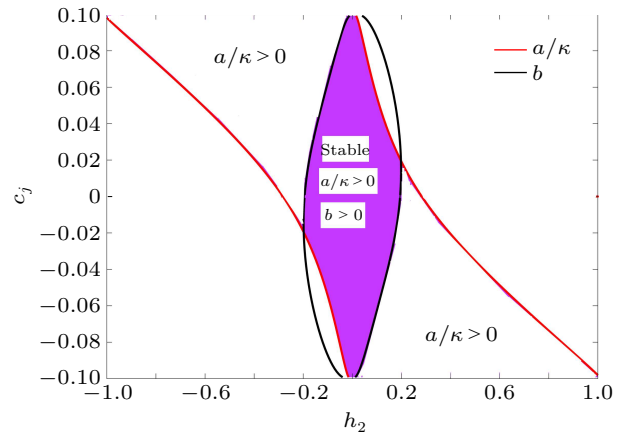


Fig. 5. The phase diagram of steady region in the h–c_j plane for the magnetic state $\theta_0 = \arcsin[(k - f_0)f_1]^{1/2}$ and $\phi_0 = \arcsin(h_2^2(k - f_0)k)^{1/2}/[2c_j^2(c_j^2 + h_2^2)]$. The phase diagram in the magnetic steady state of the equilibrium states, the equilibrium in the h–c_j plane. The red line denotes as the boundary of $a/\kappa = 0$, the black line denotes as the boundary of $b = 0$. The purple region denotes as the stable region. The related parameters are the same as in Fig. 4.

In Fig. 5 we plot the stable region with the stability conditions $b \geq 0$ and $a/\kappa \geq 0$. The red line represents $a/\kappa = 0$, and the black line represents $b = 0$. Obviously, the common purple region is the stable region. Here, the corresponding parameters are as follows: the Gilbert damping parameters $\alpha = 0.2$, $K = 1.6 \times 10^5$ J/m^3, the uniaxial anisotropic constant is $k = K/(\mu_0 M_s^2) \approx 0.2$. However, comparing Figs. 4 and 5 we find that the spin Hall effect makes the stable region of this states smaller than the above case with the increasing current.

Next, we consider the stability of the equilibrium state $\theta_0 = \pi/2$ and $\phi_0 = \pi/2$. Substituting θ_0 and ϕ_0 into the conditions of stability, we have $k_\theta = c_j$, $k_\phi = -h_y$, $l_\theta = h_y - k$, $l_\phi = c_j$, $a = \alpha(2h_y - k) - 2c_j$, $b = 4\alpha^2 c_j^2 + 4\alpha c_j(2h_y - k) + (4h_y^2 - k^2\alpha^2 - 4kh_y)$. From the stability conditions $a/\kappa \geq 0$ and $b \geq 0$ we obtain $c_j \leq \alpha(h_y - k/2)$ and $c_j \leq -[k(\alpha_1 - 1) + 2h_y]/(2\alpha)$ or $c_j \geq [k(\alpha_1 + 1) - 2h_y]/(2\alpha)$, respectively. With these results we find there are two magnetic field critical values, i.e., $h_y = k(\alpha_1 \mp 1)/(2\alpha_1)$, denoted by the point N_1 for the case $-$ and N_2 for the case $+$ in Fig. 6. For the case $-$ the stable condition is $c_j \leq [(k - 2h_y) - k\alpha_1]/2\alpha$ as the external field greater than the critical value, while $c_j \leq \alpha(h_y - k/2)$ as the external field less than the critical value, as shown in Fig. 6. For the case $+$, we obtain the stable condition, i.e., $(k(\alpha_1 + 1) - 2h_y)/(2\alpha) \leq c_j \leq \alpha(h_y - k/2)$, as well the external field is greater than the critical value, as shown in Fig. 6. With the above analysis, we adopt the parameters as follows: $\alpha = 0.2$, $K = 1.6 \times 10^5$ J/m^3, and the uniaxial anisotropic constant is $k = K/(\mu_0 M_s^2) \approx 0.2$. In Fig. 6, the red line denotes the condition $a/\kappa = 0$, i.e., $c_j = \alpha(h_y - k/2)$. The region below the red line represents $a/\kappa > 0$, while above the red line represents $a/\kappa < 0$. The blue and black lines denote the condition $b = 0$, i.e., b_1 and b_2 are shown in Fig. 6. The region which below the blue line and above the black line represents $b > 0$. By adjusting the magnitude of the external magnetic field and the current density, we can find the stable region of the equilibrium state $\theta_0 = \pi/2$ and $\phi_0 = \pi/2$.

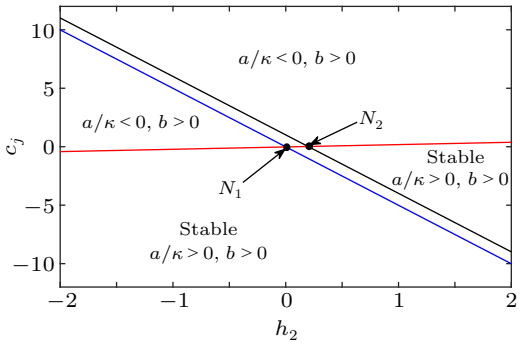


Fig. 6. The phase diagram of steady region in h–c_j plane for the magnetic equilibrium state $(\pi/2, \pi/2)$. The red line denotes as the boundary of $a/\kappa = 0$, the blue line and black line denote as the boundary of $b = 0$. Here we select the related parameters as follows: the Gilbert damping parameter $\alpha = 0.2$, $K = 1.6 \times 10^5$ J/m^3, the uniaxial anisotropic constant $k = K/(\mu_0 M_s^2) \approx 0.2$.

At last, we consider the stability of the equilibrium state $(\pi/2, 3\pi/2)$. Substituting θ_0 and ϕ_0 into the conditions of stability, we have $k_\theta = -c_j$, $k_\phi = h_y$, $l_\theta = -h_y - k$, $l_\phi = -c_j$, $a = -\alpha(2h_y + k) + 2c_j$, $b = 4\alpha^2 c_j^2 + 4\alpha c_j(2h_y + k) + (4h_y^2 - k^2\alpha^2 + 4kh_y)$. The stability conditions $a/\kappa \geq 0$ and $b \geq 0$ demand that $c_j \geq \alpha(h_y + k/2)$ and $c_j \leq -(k + k\alpha_1 + 2h_y)/2\alpha$ or $c_j \geq (-k + k\alpha_1 - 2h_y)/2\alpha$. Following the above same discussion we get the critical value of the magnetic field $h_y = -k(1 \pm \alpha_1)/(2\alpha_1)$, denoted by the point N_3 for the case $+$ and N_4 for the case $-$ in Fig. 7. For the case $-$, the stable condition becomes $c_j \geq (k\alpha_1 - k - 2h_y)/2\alpha$ as the external field less than the critical value, while the stable condition is $c_j \geq \alpha(k/2 + h_y)$ as the external field greater than the critical value. For the case $+$, the stable condition is $\alpha(k/2 + h_y) \leq c_j \leq -(k + 2h_y + k\alpha_1)/2\alpha$ as the external field less than the critical value. With the above analysis we give the stable region of the equilibrium state $(\pi/2, 3\pi/2)$ in Fig. 7, in which the blue and black lines represent the condition $b = 0$ corresponding to $c_j = -(k \pm 2h_y + k\alpha_1)/2\alpha$, respectively.

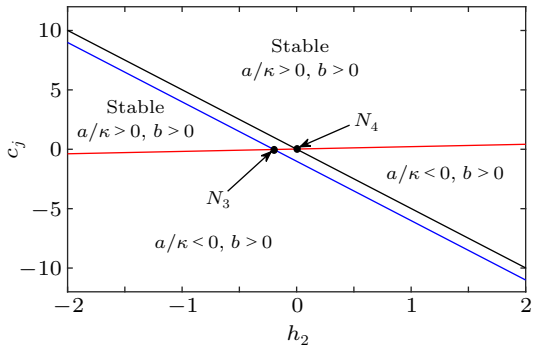


Fig. 7. The phase diagram of steady region in h–c_j plane for the magnetic equilibrium state $(\pi/2, 3\pi/2)$. The red line denotes as the boundary of $a/\kappa = 0$, the blue line and black line denote as the boundary of $b = 0$. The parameters are the same as in Fig. 6.

5. Conclusion

In this paper, we have theoretically studied the stability of magnetization in the free layer where the spin torque is induced by spin Hall effect. By linear stability analysis, we find the equilibrium states in different conditions. Without the external magnetic field, we obtain three sets of equilibrium states, among which the minimal energy state is the stable state, the maximum energy state is unstable. Controlling by the spin Hall angle and current density, we establish the phase diagrams of the stable regions. These results show that the spin Hall effect and the external magnetic filed can effectively affect the phase diagrams of stable regions.

Acknowledgments

Project supported by the Program of State Key Laboratory of Quantum Optics and Quantum Optics Devices of Shanxi University of China (Grant No. KF202203).

References

[1] Thomas L, Moriya R, Rettner C and Parkin S S P 2010 *Science* **330** 1810

[2] Slonczewski J 1996 *J. Magn. Magn. Mater.* **159** L1

[3] Berger L 1996 *Phys. Rev. B* **54** 9353

[4] Li Z D, Cui H, Li Q Y and He P B 2018 *Ann. Phys.* **388** 390

[5] Zhou Z, Zhang X, Guo Y, Zhang Y, Niu X, Ma L and Wang J 2021 *Phys. Rev. B* **103** 245411

[6] Rakhmanov A L, Sboychakov A O, Kugel K I, Rozhkov A V and Nori F 2018 *Phys. Rev. B* **98** 155141

[7] Schüler M, Murakami Y and Werner P 2018 *Phys. Rev. B* **97** 155136

[8] Wang Z Y and Sun Z Z 2018 *J. Appl. Phys.* **115** 063905

[9] Manchon A, Železný J, Miron I M, Jungwirth T, Sinova J, Thiaville A, Garello K and Gambardella P 2019 *Rev. Mod. Phys.* **91** 035004

[10] Lee K S, Lee S W, Min B C and Lee K J 2013 *Appl. Phys. Lett.* **102** 112410

[11] Kawahara T, Takemura R, Miura K, Hayakawa J, Ikeda S, Lee Y M, Sasaki R, Goto Y, Ito K, Meguro T, Matsukura F, Takahashi H, Matsuoka H and Ohno H 2008 *IEEE J. Solid-State Circuits* **43** 109

[12] Kiselev S I, Sankey J C, Krivorotov I N, Emley N C, Schoelkopf R J, Buhrman R A and Ralph D C 2003 *Nature* **425** 380

[13] Miron I M, Garello K, Gaudin G, Zermatter P J, Costache M V, Auffret S, Bandiera S, Rodmacq B, Schuhl A and Gambardella P 2011 *Nature* **476** 189

[14] Liu L, Pai C F, Li Y, Tseng H W, Ralph D C and Buhrman R A 2012 *Science* **336** 555

[15] Liu L, Lee O J, Gudmundsen T J, Ralph D C and Buhrman R A 2012 *Phys. Rev. Lett.* **109** 096602

[16] Hirsch J E 1999 *Phys. Rev. Lett.* **83** 1834

[17] Ohuchi Y, Kozuka Y, Uchida M, Ueno K, Tsukazaki A and Kawasaki M 2015 *Phys. Rev. B* **91** 245115

[18] Laurell P and Fiete G A 2018 *Phys. Rev. B* **98** 094419

[19] Beauvois K, Simonet V, Petit S, Robert J, Bourdarot F, Gospodinov M, Mukhin A A, Ballou R, Skumryev V and Ressouche E 2020 *Phys. Rev. Lett.* **124** 127202

[20] Zhou Y, Guo C, Wan C, Chen X, Zhou X, Zhang R and Song C 2020 *Phys. Rev. Appl.* **13** 064051

[21] Bazaliy Y B, Jones B A and Zhang S C 2004 *Phys. Rev. B* **69** 094421

[22] Grollier J, Cros V, Jaffrès H, Hamzic A, George J M, Faini G, Ben Y J, Le G H and Fert A 2003 *Phys. Rev. B* **67** 174402

[23] Morise H and Nakamura S 2005 *Phys. Rev. B* **71** 014439

[24] Smith N, Katine J A, Childress J R and Carey M J 2005 *IEEE Trans. Magn.* **41** 2935

[25] Slavin A N and Tiberkevich V S 2005 *Phys. Rev. B* **72** 094428

[26] Stiles M D and Miltat J 2006 *Spin Transfer Torque and Dynamics* (Berlin: Springer-Verlag) p. 225

[27] Ebels U, Houssameddine D, Firastrau I, Gusakova D, Thirion C, Dieny B and Buda-Prejbeanu L D 2008 *Phys. Rev. B* **78** 024436

[28] He P B, Wang R X, Li Z D, Liu Q H, Pan A L, Wang Y G and Zou B S 2010 *Eur. Phys. J. B* **73** 417

[29] Baronio F, Chen S, Grelu P, Wabnitz S and Conforti M 2015 *Phys. Rev. Appl.* **91** 033804

[30] Duan L, Zhao L C, Xu W H, Liu C, Yang Z Y and Yang W L 2017 *Phys. Rev. E* **95** 042212

[31] Li P, Wang L, Kong L Q, Wang X and Xie Z Y 2018 *Appl. Math. Lett.* **85** 110

[32] Wang W, Kevrekidis P G, Carretero-Gonzalez R and Frantzeskakis D J 2016 *Phys. Rev. Appl.* **93** 023630

[33] Risinggård V and Linder 2017 *Phys. Rev. B* **95** 134423

[34] Bi C, Almasi H, Price K, Newhouse-Illige T, Xu M, Allen S R, Fan X and Wang W 2017 *Phys. Rev. B* **95** 104434

[35] Shen L, Xia J, Zhang X, Ezawa M, Tretiakov O A, Liu X, Zhao G and Zhou Y 2020 *Phys. Rev. Lett.* **124** 037202

[36] Zhang J, Zhang Y, Gao Y, Zhao G, Qiu L, Wang K, Dou P, Peng W, Zhuang Y, Wu Y, Yu G, Zhu Z, Zhao Y, Guo Y, Zhu T, Cai J, Shen B and Wang S 2020 *Adv. Mater.* **32** 1907452

[37] Ye C, Li L L, Shu Y, Li Q R, Xia J, Hou Z P, Zhou Y, Liu X X, Yang Y Y and Zhao G P 2022 *Rare Metals* **41** 2200

[38] Li L, Luo J, Xia J, Zhou Y, Liu X and Zhao G 2023 *Chin. Phys. B* **32** 017506

[39] Xia J, Zhang X, Tretiakov O A, Diep H T, Yang J, Zhao G, Ezawa M, Zhou Y and Liu X 2022 *Phys. Rev. B* **105** 214402

[40] Liang X, Zhang X, Xia J, Ezawa M, Zhao Y, Zhao G and Zhou Y 2020 *Appl. Phys. Lett.* **116** 122402

[41] Shen L, Xia J, Zhao G, Zhang X, Ezawa M, Tretiakov O A, Liu X and Zhou Y 2019 *Appl. Phys. Lett.* **114** 042402

[42] Zhao G P, Wang X L, Feng Y P and Huang C W 2007 *IEEE Trans. Magn.* **43** 2908

[43] Zhao G P, Zhao L, Shen L C, Zou J and Qiu L 2019 *Chin. Phys. B* **28** 077505

[44] Zhao G P, Yang C, Xian C W and Feng Y P 2009 *Mod. Phys. Lett. B* **23** 2955

[45] Stoner E C and Wohlfarth E P 2003 *Philos. Trans. Roy. Soc. A* **27** 3475